厚生労働科学研究費補助金

障害者対策総合研究事業（感覚器障害分野）

新世代人工内耳に対応した内耳薬剤徐放技術の開発

平成23年度　総括研究報告書

研究代表者　吉　川　弥　生

平成24（2012）年3月

厚生労働科学研究費補助金

障害者対策総合研究事業

（感覚器障害分野）

新世代人工内耳に対応した内耳薬剤徐放技術の開発

平成23年度　総括研究報告書

研究代表者　吉川　弥生

平成24（2012）年　3月

目　　次

厚生労働科学研究補助金（障害者対策総合研究事業（感覚器障害分野））
統括研究報告書

新世代人工内耳に対応した内耳薬剤徐放技術の開発

研究代表者　吉川　弥生　東京大学医学部附属病院　耳鼻咽喉科・頭頸部外科
病院診療医

研究要旨

人工内耳治療には、近年になり適応拡大・両耳装用、さらには海外での人工内耳と補聴器の併用（EAS）といった大きなパラダイム・シフトが起きている。これを実現するには、埋込術後の急性期の蝸牛障害を予防する技術の開発が必須である。

本研究課題では、研究代表者らが有するバイオマテリアル技術および内耳アポトーシス予防技術を統合し、薬剤徐放機能付き人工内耳などの新たな内耳治療手技の開発を行った。

本年度は、これまでにテストしてきた薬剤徐放用人工材料の欠点を克服する新たな素材として３つの候補の比較実験を行い、最終的に MPC（2-メタクリロイル オキシエチルホスホリルコリン）ポリマーを選定、動物実験用薬剤徐放電極を作成した。電極特性の基礎実験、動物実験を実施し海外（オーストラリア）の人工内耳製造会社と商品化に向けた協議を進めた。

分担研究者
坂本　幸士　東京大学医学部附属病院　耳鼻咽喉科・頭頸部外科　講師
狩野章太郎　東京大学医学部附属病院　耳鼻咽喉科・頭頸部外科　特任講師
松本　有　東京大学医学系研究科　臨床医工学部門　特任研究員
樫尾　明憲　東京大学医学部附属病院　耳鼻咽喉科・頭頸部外科　助教

A．研究目的

新世代人工内耳の発展

人工内耳は 20 世紀最高の発明とも言われ、最も成功した人工臓器のひとつである。1970 年代の実用化以降、単チャンネルからマルチチャンネルへ、スピーチプロセッサの IC 化といった様々な改良がなされてきたが、近年になり大きなパラダイム・シフトが起きている。それは、人工内耳自体の性能向上に沿った中等度難聴への適応拡大・両耳装用、さらには人工内耳と補聴器の併用（EAS）などに代表される「人工内耳治療の普遍化」である（Van de Heyning 2010）。EAS は欧州ではすでに 10 年前より臨床での使用が始まっているが、日本でも本年 12 月 9 日に厚生労働省「高度医療評価会議」で承認され、普及への第１歩を踏み出した。

しかしながら、こうした新世代人工内耳に対応した内耳保護技術は必ずしも充分ではない。EAS

を行うためには残存聴力の温存が必須であるが、電極挿入により起こる内耳組織破壊・繊維化などのために不可逆的に喪失してしまうことが多い(Nadol 1997 など)。したがってより安全で低侵襲な人工内耳手術術式を開発するとともに、手術時には繊維化を防ぎ、蝸牛細胞を保護・再生する薬剤を内耳局所に投与することが望まれている。

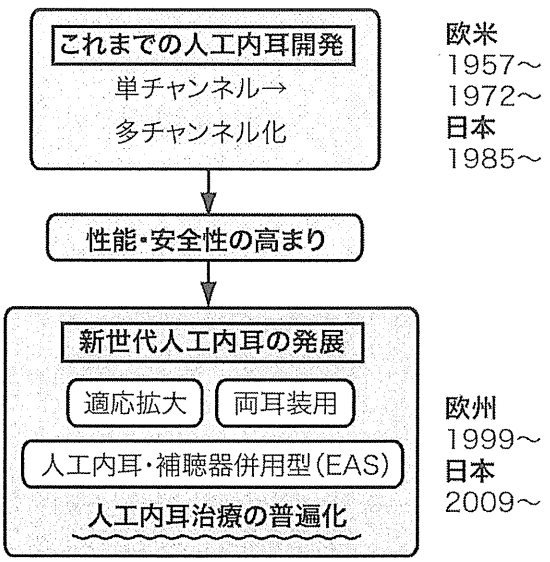

図１　人工内耳の発展

人工内耳を利用した薬剤投与技術の開発が急務である

人工内耳からの薬剤投与に関しては現在世界的に熾烈な競争が繰り広げられているが、浸透圧ポンプなどを使うと装置が巨大化してしまうことや、効果の高い薬剤が入手できないといった理由からいずれも学会報告レベルに留まっている。

研究代表者はこれまで所属していたテキサス大学、京都大学で人工内耳の感染予防加工や低侵襲手術法の開発を行い(Med-El 社との共同研究)、内耳薬剤徐放の種々の技法を習得した。IGF-1・ハイドロゲル徐放製剤は動物実験で高い効果が得られ、突発性難聴に対する臨床第 I/II 相試験では５割に効果を認めた（BMC Medicine 2010, 8:76）。また、東京大学ではアポトーシス予防に関して基礎研究(Someya 2009 PNAS)、全身投与(Kashio 2007, J Neurosci Res)を通して技術を確立しており、本研究ではこの両者の技術を統合して内耳薬剤徐放機能を備えた低侵襲型人工内耳を開発、人工内耳埋込時に起きる組織損傷を極限まで抑える技術を開発する。

さらにこの技術が完成すれば、人工内耳治療に

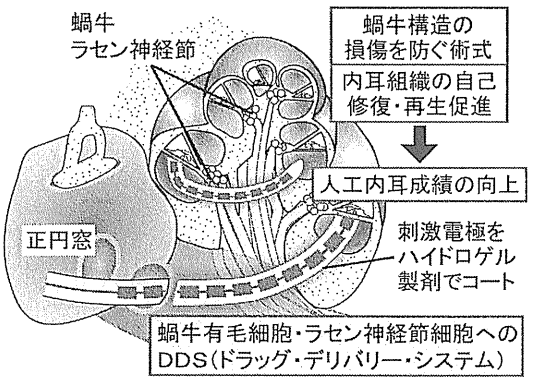

図２　本計画の概念図

限らず突発性難聴や進行性難聴などの様々な内耳疾患の普遍的な治療法として応用が期待できると考えられた。

昨年度（研究初年度）の展開

昨年度は薬剤徐放コート層としてゼラチン・ハイドロゲル（図３）を使用したプロトタイプ電極を製作し、基礎実験および動物実験を行った。(図４)

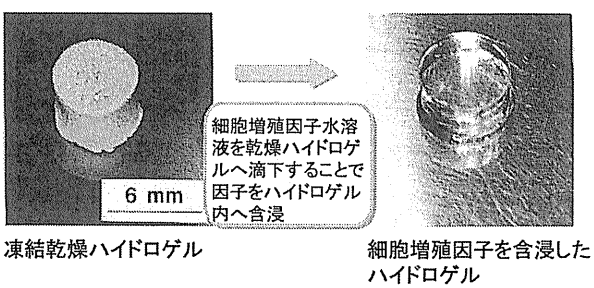

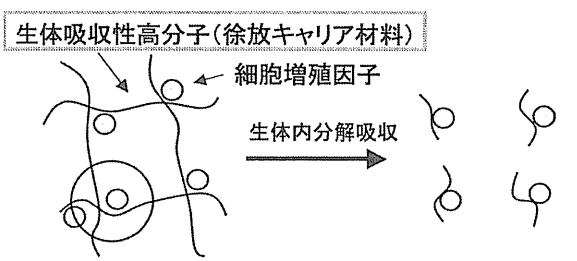

ハイドロゲル徐放システムは優れた薬剤保持能と徐放能を持ちゲル量に応じて薬剤徐放速度と徐放時間を制御でき、中耳・内耳での炎症反応は認められず低刺激性であるため内耳用徐放製剤として使用可能ことが確認できた。

しかしダミー電極を挿入した際にハイドロゲル層が剥奪する事故が高い頻度で発生すること、また、ハイドロゲル原料が豚皮由来であり生物学的製剤であるため潜在的な感染症リスクがあること、この２点を考慮して新たな薬剤徐放物質の探索が必要となった。

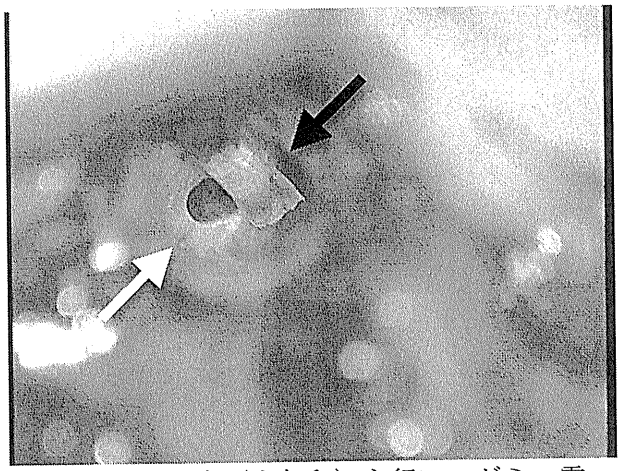

図４　蝸牛開窓（白矢印）を行い、ダミー電極（黒矢印）を挿入

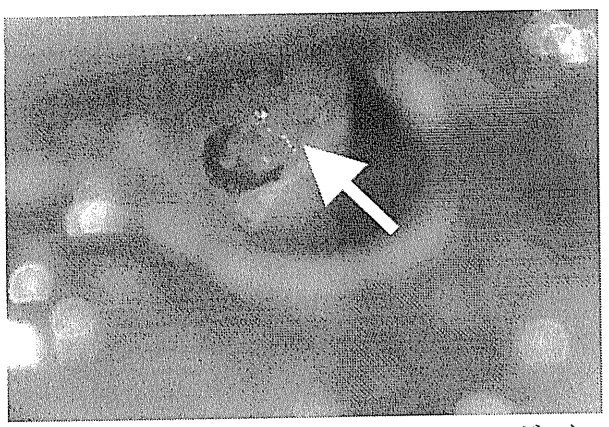

図５　薬剤徐放層（ゼラチン・ハイドロゲル）の剥脱（白矢印）

B．研究方法

・最適材料の選定

以下の３つの材料に関して検討を加えた。

① Tetra-PEG gel（Kurakazu 2010、東大工学部（マテリアル工学専攻）酒井崇匡助教）

② ナノミセル型DDS　（Nishiyama 2003、東大医工連携　片岡一則教授）

③MPCポリマーゲル（Kihara 2003、東大工学部（先端バイオデバイス工学）石原教授、金野准教授）

①は軟骨再生材料として前臨床試験中、②のナノミセル型DDSはダハプラチン内包ナノミセル抗がん剤（ナノプラチン）として Phase III 試験中、③は国産で初めて承認された埋込型補助人工心臓「エバハート」の血栓予防のための表面コーティングとして市販され、それぞれ臨床応用されている。

・徐放性能・安全性・耐久性テスト

上の選定作業で選んだ材料を用いてダミー人工内耳を作成、以下の試験を行って内耳薬剤徐放材料としての性能を検証した。ベースとなる人工内耳にはコクレア社（オーストラリア）Nucleus シリーズを使用した。

<u>電極コーティングの特性検査</u>

光学顕微鏡・電子顕微鏡検査

<u>通電検査</u>

音響インピーダンス検査
サイクリックボルタンメトリー
電気化学インピーダンス
スペクトロスコピー
繰り返し通電検査
一過性電位測定

<u>耐損傷検査</u>（電子顕微鏡）

埋め込み術後検査

・モルモット蝸牛損傷予防実験

1．人工内耳電極（コート済みの物およびコートなしの物）を EOG 滅菌する。

2．モルモット側頭部に耳後切開を置いて耳胞を開放、蝸牛開窓を置きそこからダミー電極を挿入し、コートの有無による挿入の容易さを比較する。

3．術前、術直後、３、７、14、28、56 日後に ABR を測定する。

４．８週後に蝸牛を回収し中耳および内耳の組織学的検査を行う。

（倫理面への配慮）

動物実験に関しては、本学の動物実験に関する倫理委員会の承認のもとに、動物愛護に十分配慮した上で行う。ヒト側頭骨を使用する場合は、人権擁護上の配慮を十分に行った上で研究を実施する。

C．研究結果

・最適材料の選定

・Tetra-PEG gel

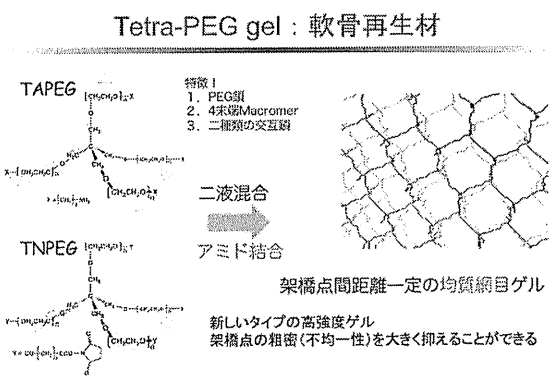

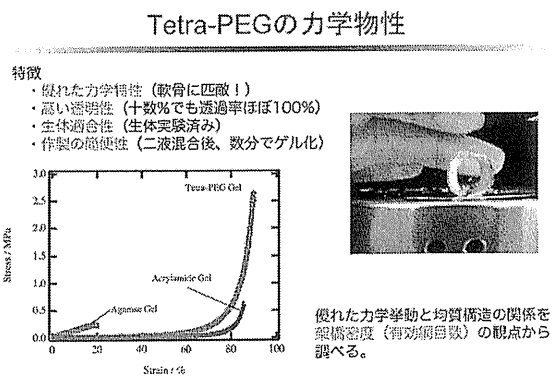

・硬度が高く、人工内耳電極コートに適さない→断念

Tetra-PEG ゲルは軟骨の代替材料になりうる優れた力学特性を持ち、作成も簡便であるが、硬度が高すぎるために人工内耳電極被覆剤としては不適であった。

・ナノミセル

ナノミセルを用いた薬剤徐放は、疎水性ポリマーを内包するためステロイドなどの疎水性薬剤の徐放に最適と考えられたが、粒子状のため人工内耳の電極コートには使うことができなかった。

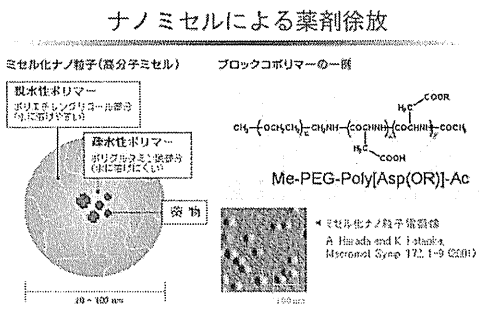

・粒子状のため人工内耳の電極コートに適さない

・MPCポリマーゲル

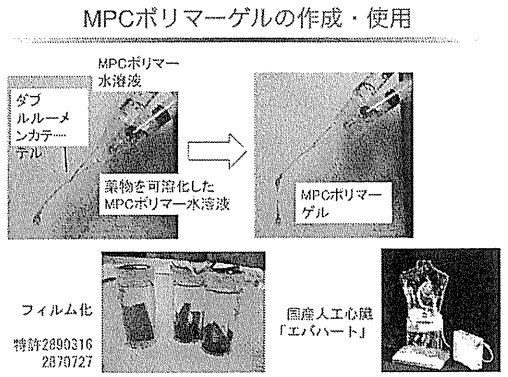

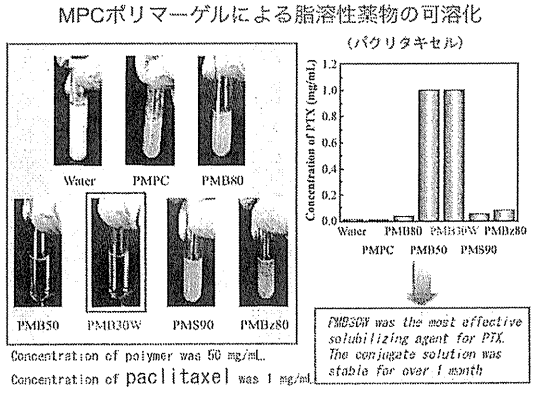

MPC polymer は国産補助人工心臓「エバハート」の表面被覆素材として承認済みであり、平成２３年４月からは国内の市販も始まっている。また、MPC ポリマーをコーティングすることにより血小板等の蛋白質の吸着を防ぐことができるため、コンタクトレンズケア製品、抗血栓性を主目的にした人工透析やカテーテル等の医療デバイスのコーティング材料（リピジュア®-CM）として注目されている。ポリマー水溶液と重合剤の

2液を混合させて作るため、薄膜フィルム化および薬剤含浸がきわめて容易である。

以上よりゼラチン・ハイドロゲルに代わる新たな人工内耳徐放コート剤としてMPCポリマーを選定し、以降の実験を行った。

・齧歯類モデルでの動物実験

動物用ダミー電極を用い、MPC polymerを使用した内耳挿入実験を実施。MPC polymerでコートした電極がモルモット内耳に強い炎症反応を惹起しないこと、また、非コート電極に比べて外装が親水性であるため電極挿入が容易になることを確認した。(前臨床試験用の基礎データ)。

D．考察

本研究では、昨年度の段階でゼラチン・ハイドロゲルで被覆した人工内耳ダミー電極が内耳用徐放製剤として使用可能で、ゲル量に応じて薬剤徐放速度と徐放時間を制御できることが確認できた。動物実験では人工内耳埋込術時の蝸牛損傷予防に大きな効果を発揮することがわかり、実用化に向けて人工内耳メーカーを含め協議中であったが、実験中、ダミー電極を挿入した際に電極からハイドロゲル層が剥奪する事故が発生しうることが判明した。O_3（オゾン）処理を行ってゲル層とシリコンの結合を強固にしようとしたが事故が減らず、薬剤徐放電極の実用化は困難かと思われた。

そのためハイドロゲルに代わる新たな徐放材料を検討し、MPC（2-メタクリロイル オキシエチルホスホリルコリン）ポリマーを選定した。MPC polymerはすでに医療用コーティング材料として厚労省より承認、国内外で市販されているため実用化・臨床応用が容易であり、本研究でも動物実験で性能を確認することができた。

今後は徐放型人工内耳電極として、知的財産化・特許申請および実用化を進めていく予定である。

E．結論

本研究課題では、研究代表者らが有するバイオマテリアル技術および内耳アポトーシス予防技術を統合し、薬剤徐放機能付き人工内耳などの新たな内耳治療手技の開発を行った。今後、徐放性能の最適化および臨床試験への準備を進めて行く。

F．健康危険情報

現時点では、ヒトにおける健康危険に関する情報は得られていない。

G．研究発表

1．論文発表

Kashio A, Ito K, Kakigi A, Karino S, Iwasaki S, Sakamoto T, Yasui T, Suzuki M, Yamasoba T. Carhart notch 2-kHz bone conduction threshold dip: a nondefinitive predictor of stapes fixation in conductive hearing loss with normal tympanic membrane. *Arch Otolaryngol Head Neck Surg.* 137:236-240,2011

Karino S, Philip H. Smith , Tom C. T. Yin, Philip X. Joris. Axonal Branching Patterns as Sources of Delay in the Mammalian Auditory Brainstem: A Re-Examination. *J. Neurosci.* 31: 3016-3031, 2011

Sakamoto T, Kakigi A, Kashio A, Kanaya K, Suzuki M, Yamasoba T. Evaluation of the Carhart effect in congenital middle ear malformation with both an intact external ear canal and a mobile stapes footplate. *ORL J Otorhinolaryngol Relat Spec.* 73:61-7,2011

Suzukawa K, Kondo K, Kanaya K, Sakamoto T, Watanabe K, Ushio M, Kaga K, Yamasoba T, Age-related changes of the regeneration mode in the mouse peripheral olfactory system following olfactotoxic drug methimazole-induced damage. *J Comp Neurol.* 519:2154-2174,2011

松本　有、野本貴大、藤加珠子、片岡一則．生体内リアルタイム共焦点顕微鏡．*Drug Delivery System* 26(5)：535-539，2011

2．学会発表

ARO　2011.2.19-23　Baltimore

Urokinase-type plasminogen activator attenuates hair cell damage induced by aminoglycoside.

Kashio A, Sakamoto T, Kakigi A, Kondo K, Yamasoba T

第 27 回日本 DDS 学会　2011.6.9-10　東京

シスプラチン内包高分子ミセルによる内耳障害軽減効果

馬場美雪、松本有、カブラルオラシオ、西山伸宏、片岡一則、山岨達也

第 6 回日本小児耳鼻咽喉科学会　2011.6.16-17　さいたま市

当科における先天性サイトメガロウイルス感染症児に対する人工内耳の成績

樫尾明憲、安達のどか、安井拓也、尾形エリカ、赤松裕介、坂田英明、山岨達也

再手術を要した小児人工内耳症例の検討

斉藤真紀、樫尾明憲、狩野章太郎、尾形エリカ、赤松裕介、安達のどか、浅沼聡、坂本幸士、柿木章伸、山岨達也

当科における重複障害児に対する人工内耳成績

赤松裕介、尾形エリカ、樫尾明憲、安井拓也、安達のどか、浅沼聡、山岨達也

第 60 回高分子討論会　2011.9.28-30　岡山市

PEG-detachable polyaspartamide derivative block copolymer bearing stearoyl moieities for in vivo siRNA delivery

Kim HJ, Oba M, Pittella F, Nomoto T, Cabral H, Matsumoto Y, Miyata K, Nishiyama N, Kataoka K

APSCI 2011　10.25-28　Daegu

Cochlear implant in children with GJB2 gene mutation

Kashio A, Akamatsu Y, Ogata E, Adachi N, Yasui T, Karino S, Sakamoto T, Kakigi A, Iwasaki I, Yamasoba T

日本聴覚医学会 2011.10.28　福岡

雑音負荷時の子音聴取－信号音源と雑音音源の空間的配置との関連

狩野章太郎、赤松裕介、越智篤、山岨達也

Seoul Nanohealth 2011 Symposium 2011.11.17-18 Seoul, Korea

In Situ Monitoring of Drug Delivery Systems Using Intravital Real-time Confocal Laser Scanning Microscopy

Nomoto T, Matsumoto Y, Miyata K, Oba M, Fukushima S, Cabral H, Murakami M, Nishiyama N, Kataoka K

第 21 回 日本耳科学会総会・学術講演会　2011.11.24-26 宜野湾

アポトーシス抑制蛋白 PTD-FNK を用いた内耳タンパク治療　<公募シンポジウム>

樫尾明憲

生体内リアルタイム共焦点顕微鏡と蝸牛イメージングへの展開

松本有、狩野章太郎、吉川弥生、奥野妙子、片岡一則、山岨達也

外耳道閉鎖症の術後聴力に影響を及ぼす因子に関する多重ロジスティッ回帰分析による検討

坂本幸士、樫尾明憲、安井拓也、狩野章太郎、柿木章伸、山岨達也

11th Japan-Taiwan Conference on Otolaryngology-Head and Neck Surgery　2011.12.8-9　Kobe

Symposium: Novel technologies to prevent from inner ear damage. Nanotechnology and PTD technology

Yamasoba T, Kashio A, Baba M.

The 11th US-Japan Symposium on Drug Delivery Systems　2011.12.19-20　Hawaii,USA

Clinical Course and Features of Fatal Intersititial Pneumonitis Induced by PEGylated Liposomal Doxorubicin (PLD) and Analysis of PLD-Induced Lung Injury Using Real-Time Intravital Microscope

Matsumoto Y, Arimoto T, Oda K, Kawana K, Yano T, Taketani Y, Matsumoto Y, Nomoto T, Toh K, Kataoka K

Intravital Real-Time Confocal Laser Scanning Microscopy for In Situ Evaluation of Nanocarriers

Matsumoto Y, Nomoto T, Toh K, Miyata K, Cabral H, Christie RJ, Matsumoto Y, Nishiyama N, Yamasoba T, Kataoka K

H. 知的財産権の出願・登録状況

1. 特許取得

なし

2. 実用新案登録

なし

3. その他

なし

研究成果の刊行に関する一覧表

雑誌

発表者氏名	論文タイトル名	発表誌名	巻号	ページ	出版年
Kashio A, Ito K, Kakigi A, Karino S, Iwasaki S, Sakamoto T, Yasui T, Suzuki M, Yamasoba T.	Carhart notch 2-kHz bone conduction threshold dip: a nondefinitive predictor of stapes fixation in conductive hearing loss with normal tympanic membrane.	*Arch Otolaryngol Head Neck Surg.*	137	236-240	2011
Karino S, Philip H. Smith , Tom C. T. Yin, Philip X. Joris.	Axonal Branching Patterns as Sources of Delay in the Mammalian Auditory Brainstem: A Re-Examination.	*J. Neurosci*	31	3016-3031	2011
Sakamoto T, Kakigi A, Kashio A, Kanaya K, Suzuki M, Yamasoba T	Evaluation of the Carhart effect in congenital middle ear malformation with both an intact external ear canal and a mobile stapes footplate.	*ORL J Otorhinolaryngol Relat Spec.*	73	61-7	2011
Suzukawa K, Kondo K, Kanaya K, Sakamoto T, Watanabe K, Ushio M, Kaga K, Yamasoba T	Age-related changes of the regeneration mode in the mouse peripheral olfactory system following olfactotoxic drug methimazole-induced damage.	*J Comp Neurol.*	519	2154-2174	2011
松本　有、野本貴大、藤加珠子、片岡一則.	生体内リアルタイム共焦点顕微鏡.	*Drug Delivery System*	26	535-539	2011

ORIGINAL ARTICLE

Carhart Notch 2-kHz Bone Conduction Threshold Dip

A Nondefinitive Predictor of Stapes Fixation in Conductive Hearing Loss With Normal Tympanic Membrane

Akinori Kashio, MD; Ken Ito, MD; Akinobu Kakigi, MD; Shotaro Karino, MD; Shin-ichi Iwasaki, MD; Takashi Sakamoto, MD; Takuya Yasui, MD; Mitsuya Suzuki, MD; Tatsuya Yamasoba, MD

Objective: To evaluate the significance of the Carhart notch (a 2-kHz bone conduction threshold dip [2KBD]) in the diagnosis of stapes fixation by comparing its incidence among ears with various ossicular chain abnormalities.

Design: Retrospective study.

Setting: University hospital.

Patients: A total of 153 ears among 127 consecutive patients with a congenital ossicular anomaly or otosclerosis.

Main Outcome Measures: The 2KBD depth was defined as the threshold at 2 kHz minus the mean of thresholds at 1 and 4 kHz. The presence of 2KBD (depth, ≥10 dB), 2KBD depth, relationship between 2KBD depth and air-bone gap, and 2-kHz bone conduction recovery after operation were evaluated in a stapes fixation group (which included cases of otosclerosis and congenital stapes fixation), an incudostapedial joint detachment group, and a malleus or incus fixation group.

Results: A 2KBD was present in 32 of 102 stapes fixation ears (31.4%), 5 of 19 incudostapedial joint detachment ears (26.3%), and 6 of 20 malleus or incus fixation ears (30.0%) (12 ears had other diagnoses). The mean (SD) 2KBD depths were 17.3 (5.2) dB in the stapes fixation group, 18.5 (2.2) dB in the incudostapedial joint detachment group, and 16.3 (2.1) dB in the malleus or incus fixation group. No statistically significant differences were noted among these 3 groups. No correlation was noted between 2KBD depth and air-bone gap extent. Recovery of 2-kHz bone conduction threshold in the stapes fixation group was less than that in the other 2 groups.

Conclusion: Incidence of 2KBD was similar among the stapes fixation, incudostapedial joint detachment, and malleus or incus fixation groups, implying that 2KBD is not a useful predictor of stapes fixation.

Arch Otolaryngol Head Neck Surg. 2011;137(3):236-240

Author Affiliations:
Department of Otolaryngology, Faculty of Medicine, University of Tokyo (Drs Kashio, Kakigi, Karino, Iwasaki, Sakamoto, Yasui, and Yamasoba), and Department of Otolaryngology, Teikyo University School of Medicine (Dr Ito), Tokyo, and Department of Otolaryngology–Head and Neck Surgery, Sakura Medical Center, University of Toho, Chiba (Dr Suzuki), Japan.

In 1950, Carhart[1] reported bone conduction threshold elevation of approximately 2 kHz among patients with otosclerotic lesion–induced stapes ankylosis that disappeared after stapes surgery. Since then, this deceptive 2-kHz bone conduction threshold dip (2KBD) without inner ear damage has become a well-known indicator of stapes fixation (Carhart notch). However, results of studies[2-9] have suggested that elevation in bone conduction thresholds between 1 and 4 kHz can be caused by various factors that affect the conductive mechanism of the middle ear. In fact, it is not uncommon to encounter cases of Carhart notch in which hearing loss is caused by detachment of the incudostapedial joint. For Carhart notch to be used as a preoperative predictor of stapes fixation, it should be shown that the notch exists with stapes fixation but not with other ossicular chain disorders, such as disconnection; however, few clinical investigations have assessed this issue. In the present study, we evaluated the significance of 2KBD depth, defined as the threshold at 2 kHz minus the mean of thresholds at 1 and 4 kHz, in diagnosing various ossicular chain abnormalities in the setting of a normal tympanic membrane.

METHODS

We studied 153 ears among 127 consecutive patients who had a congenital ossicular anomaly or otosclerosis that was confirmed during surgery between January 1997 and December 2007 at the University of Tokyo Hospital, Tokyo, Japan. On the basis of the diagnosis made during surgery, we assigned these ears to the following 3 groups:

Table 1. Postoperative Diagnosis, Age, and Preoperative Air and Bone Conduction Thresholds Among Patients With the Various Pathologic Conditions

Postoperative Diagnosis	No. of Ears	Mean (SD)		
		Patient Age, y	ACT, dB	BCT, dB
Stapes fixation	102	48 (15)	58.3 (15.1)	26.3 (11.0)
Incudostapedial joint detachment	19	26 (17)	54.0 (11.9)	15.8 (7.0)
Malleus or incus fixation	20	24 (22)	56.8 (13.5)	19.2 (12.4)
Other	12	22 (16)	65.1 (8.4)	17.2 (12.5)

Abbreviations: ACT, air conduction threshold; BCT, bone conduction threshold.

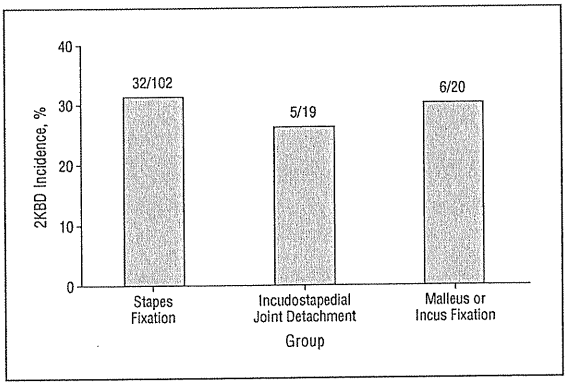

Figure 1. Incidence of 2-kHz bone conduction threshold dip (2KBD) among various pathologic conditions.

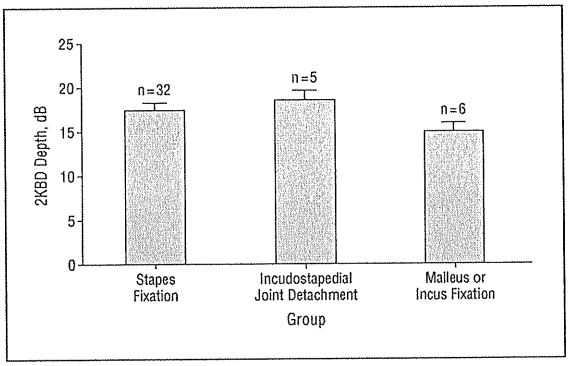

Figure 2. Depth of 2-kHz bone conduction threshold dip (2KBD) among various pathologic conditions. Error bars indicate standard error.

Table 2. Age-Related 2-kHz Bone Conduction Threshold Dip (2KBD)–Positive Rates

Age Group, y	Postoperative Diagnosis	No.	2KBD Positive
0-29	Stapes fixation	8	1
	Incudostapedial joint detachment	12	2
	Malleus or incus fixation	15	5
	Total, No. (%)	**35**	**8** (22.9)
30-59	Stapes fixation	70	20
	Incudostapedial joint detachment	6	2
	Malleus or incus fixation	2	0
	Total, No. (%)	**78**	**22** (28.2)
≥60	Stapes fixation	24	11
	Incudostapedial joint detachment	1	1
	Malleus or incus fixation	3	1
	Total, No. (%)	**28**	**13** (46.4)

a stapes fixation group (which included cases of otosclerosis and congenital stapes fixation), an incudostapedial joint detachment group, and a malleus or incus fixation group. The medical records of these patients were retrospectively reviewed. Stapes fixation was observed in 102 ears (including 15 ears with congenital fixation), incudostapedial joint detachment without stapes fixation in 19 ears, and malleus or incus fixation without stapes fixation in 20 ears. The other 12 ears (including a combination of incudostapedial joint detachment and malleus or incus fixation or obstruction of the oval window) could not be classified into the aforelisted groups and were excluded from the analysis. The patients ranged in age from 6 to 72 years (mean [SD] age, 40 [20] years). Postoperative diagnoses and the mean age and mean preoperative air and bone conduction thresholds (at 0.5, 1, and 2 kHz) are given in **Table 1**. Patients in the stapes fixation group were significantly older than those in the other 2 groups. No significant differences were noted among the 3 groups in preoperative air or bone conduction thresholds.

For audiometric evaluation, we measured air conduction thresholds at 0.125, 0.25, 0.5, 1, 2, 4, and 8 kHz. Bone conduction thresholds were measured at 0.5, 1, 2, and 4 kHz. Pure-tone audiometry was performed more than once on various days before surgery. The 2KBD was considered present when the bone conduction threshold at 2 kHz exceeded the mean of thresholds at 1 and 4 kHz by at least 10 dB. The 2KBD depth was calculated by subtracting the mean of thresholds at 1 and 4 kHz from the bone conduction threshold at 2 kHz.

Values were recorded as the mean (SD) unless indicated otherwise. Statistical analyses used χ^2 test, Wilcoxon signed rank test, and 1-way analysis of variance with Bonferroni post hoc test.

RESULTS

The 2KBD was detected in 32 of 102 ears (31.4%) in the stapes fixation group, 5 of 19 ears (26.3%) in the incudostapedial joint detachment group, and 6 of 20 ears (30.0%) in the malleus or incus fixation group (**Figure 1**). The mean 2KBD depths were 17.3 (5.2) dB in the stapes fixation group, 18.5 (2.2) dB in the incudostapedial joint detachment group, and 16.3 (2.1) dB in the malleus or incus fixation group (**Figure 2**). No statistically significant differences were noted in 2KBD incidence or 2KBD depth among the 3 groups.

Table 2 gives age-related dip-positive rates. There were no significant differences in percentages of dip-positive cases among the different age groups.

Figure 3 shows the relationship between 2KBD depth and air-bone gap, indicating no correlation between the 2 variables. No apparent differences were observed among the 3 groups.

Table 3 gives 2-kHz bone conduction thresholds before and after surgery, as well as improvements obtained by surgery. Of 102 ears in the stapes fixation group, 3 ears were excluded in which ossicular reconstruction could not be performed. Of 19 ears in the incudostapedial joint detachment group, 1 was excluded because the patient dropped out during the postoperative follow-up period. Improvement in 2-kHz

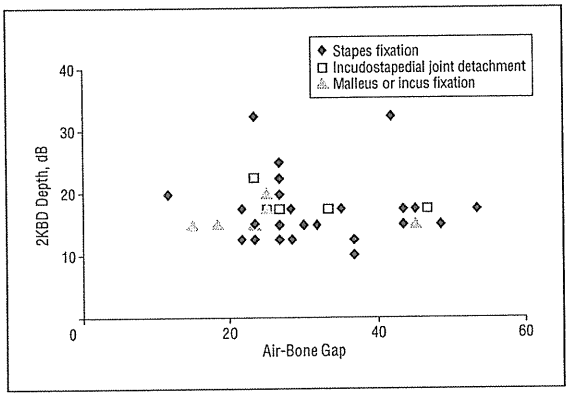

Figure 3. Relationship between 2-kHz bone conduction threshold dip (2KBD) depth and air-bone gap (r=0.34).

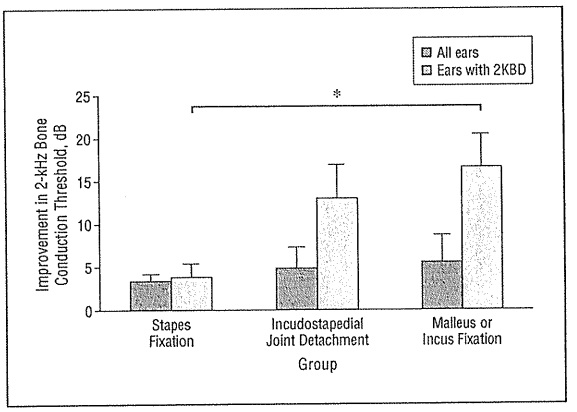

Figure 4. Postoperative recovery of 2-kHz bone conduction thresholds. Error bars indicate standard error, and the asterisk indicates a significant difference ($P<.05$, Bonferroni post hoc test). 2KBD indicates 2-kHz bone conduction threshold dip.

Table 3. Preoperative and Postoperative 2-kHz Bone Conduction Thresholds and Recovery

Postoperative Diagnosis	No. of Ears	2-kHz Bone Conduction Threshold, Mean (SD), dB		
		Preoperative	Postoperative	Recovery
Stapes fixation				
Total	99	35.0 (1.3)	31.2 (1.4)	4.6 (1.0)
2KBD positive	30	41.3 (2.0)	37.0 (2.8)	4.3 (1.9)
Incudostapedial joint detachment				
Total	18	22.2 (2.5)	16.9 (2.7)	5.6 (2.9)
2KBD positive	4	35.0 (5.3)	20.0 (6.2)	15.0 (4.7)
Malleus or incus fixation				
Total	20	26.5 (3.9)	20.1 (3.6)	6.3 (3.9)
2KBD positive	6	41.7 (7.8)	22.5 (7.7)	19.2 (4.6)

Abbreviation: 2KBD, 2-kHz bone conduction threshold dip.

bone conduction thresholds among the stapes fixation group was less than that among the other 2 groups; the difference between the 2KBD-positive stapes fixation group and the 2KBD-positive malleus or incus fixation group was statistically significant ($P<.05$, Bonferroni post hoc test) (**Figure 4**).

COMMENT

PREDICTIVE ABILITY OF CARHART NOTCH AND ITS UNDERLYING MECHANISMS

Acute or chronic otitis media associated with perforation of the tympanic membrane and otitis media with effusion can be diagnosed easily; however, in patients with normal tympanic membrane, sufficient information is needed to diagnose the cause of hearing loss. An audiological feature of 2KBD, Carhart notch, is widely known and is traditionally believed to suggest stapes fixation[10]; however, few investigations have verified its usefulness. In the present study, we evaluated the significance of Carhart notch in predicting stapes fixation and found that 2KBD was ineffective as a predictive tool. Incidence of Carhart notch was almost identical among the stapes fixation, incudostapedial joint detachment, and malleus or incus fixation groups. Otologic surgeons should be aware of this fact and should be ready to adapt their procedures according to pathologic findings during surgery.

Supporting our present findings that Carhart notch is not specific to stapes fixation, bone conduction threshold elevation between 1 and 4 kHz has also been reported in various pathologic conditions that affect the conductive mechanism of the middle ear. This phenomenon has been described in fluctuations of otitis media with effusion,[2,11-13] chronic otitis media,[5,6,14-17] experimental creation of artificial conductive impairment by loading the tympanic membrane,[8,18,19] occlusion of the round window or oval window,[8,9] and disarticulation of the incudostapedial joint.[9,20] Bone conduction threshold elevation has been reported principally between 1 and 4 kHz, with the largest being at 2 kHz.[2,5,7,21]

Bone conduction thresholds do not always represent a pure estimate of cochlear reserve, as many components are involved in bone conduction. The most important physical phenomena are believed to be (1) sound radiation into the ear canal, (2) inertial motion of the middle ear ossicles, and (3) compression and expansion of the bone encapsulating the cochlea.[22,23] Ossicular chain deficiencies are closely related to these components. A change in the ossicular chain may result in less inertial motion energy transmitted into the inner ear and can cause impedance mismatch between the inner ear and the ossicular system, modifying (decreasing or increasing) the loss of bone-conducted sound pressure from the vestibule to the footplate. It is reported that the middle ear does not contribute to perception of bone conduction sound at frequencies lower than 1 kHz.[8,20,24] At higher frequencies, the middle ear can affect bone conduction. Using human cadaver heads, Stenfelt[20] reported that motion of the stapes with bone conduction sounds was decreased by 5 to 10 dB between 1.2 and 2.7 kHz after the incudostapedial joint was severed. Using cats, Kirikae[8] reported a decrease in response at frequencies between 1 and 3 kHz after fixation of the stapes. With an intact ossicular chain, resonance frequency of the ossicular vibration with bone conduction stimulation is close to 1.5

kHz,[20] which explains 2-kHz bone conduction threshold elevation in ossicular deficiency. Therefore, although the underlying mechanisms may differ, 2-kHz bone conduction threshold elevation may well occur in various impairments of the ossicular chain, including stapes fixation, incudostapedial joint detachment, and malleus or incus fixation. The reason for this phenomenon seems complex, but oversimplification is inappropriate; further fundamental studies are needed to clarify its mechanism.

AGE-RELATED EFFECTS OF 2KBD

The mean age of patients in the stapes fixation group was significantly older than that of patients in the incudostapedial joint detachment group and the malleus or incus fixation group. In our cohort, patients in the latter 2 groups with normal tympanic membranes were mainly young adults or children with congenital malformations of the ossicular chain. This may explain the younger mean ages of these groups. Aging raises bone conduction thresholds at high frequencies, and elevation of 4-kHz bone conduction thresholds results in underestimation of potential 2KBD depths in older patients with stapes fixation. However, in our series, no significant differences were noted in 2KBD incidence among age groups. This suggests that age differences among the 3 study groups did not affect 2KBD incidence.

2KBD DEPTH AND 2-KHZ BONE CONDUCTION THRESHOLD RECOVERY AFTER SURGERY

Several investigations have focused on 2KBD, but its definitive criteria have not yet been established. However, previously reported mean 2KBD depths in otosclerosis ranged from 2.4 to 12.5 dB.[20,24,25] These studies included all cases and not just those classified as dip positive by certain criteria. The overall mean 2KBD depth, including dip-negative cases, was 8.5 dB in our stapes fixation group, which is within the range previously reported. For the 2KBD-positive cases, all 3 groups showed similar depths. These results suggest that an apparent elevation in bone conduction thresholds caused by a middle ear deficiency is similar regardless of the cause. Moreover, no correlation was observed between air-bone gap and 2KBD depth, suggesting that the depth may not be influenced by the degree of middle ear deficiency.

Carhart[1] originally reported postoperative bone conduction improvements of 5 dB at 500 Hz, 10 dB at 1 kHz, 15 dB at 2 kHz, and 5 dB at 4 kHz. Ginsberg et al[21] confirmed the finding of optimal bone conduction improvement at 2 kHz. Åwengen[25] showed an improvement of 4 to 12 dB for bone conduction at 2 kHz in otosclerosis after stapedectomy. In our series, the mean recovery of 2-kHz bone conduction was 4.6 to 6.3 dB, and the value was 4.3 to 19.2 dB when we limited the analysis to only dip-positive cases. Recovery trends in the stapes fixation group were worse than those in the other 2 groups. Gerard et al[26] proposed that there is less postoperative improvement in bone conduction with increasing age; this suggests that the aging cochlea is more susceptible to surgical damage. Because the mean age of patients was significantly older in the stapes fixation group, this may have influenced their recovery. When we evaluated 33 younger patients (about one-third of the group; mean age, 33 years) from the stapes fixation group, the overall 2KBD recovery was 7.9 (1.8) dB, which was comparable to that of the other 2 groups. Surgical procedures used in stapes surgery are more invasive and involve opening of the inner ear. Cook et al[27] reported a weak ($r=0.28$) but significant ($P<.05$) correlation between bone conduction recovery at 2 kHz and air conduction recovery after stapes surgery. We also investigated this issue and found that bone conduction recovery at 2 kHz had a weak correlation with the mean air conduction recovery ($r=0.38$, $P<.05$) but observed that preoperative air-bone gap and 2-kHz bone conduction threshold recovery had no significant correlation ($r=-0.11$, $P>.05$). These facts imply that air and bone conduction threshold elevations are related somewhat but that the underlying mechanisms of these phenomena may not be simple.

Submitted for Publication: March 29, 2010; final revision received September 10, 2010; accepted October 18, 2010.

Correspondence: Ken Ito, MD, Department of Otolaryngology, Teikyo University School of Medicine, 2-11-1 Kaga Itabashi-ku, Tokyo, Japan (itoken-tky@umin.ac.jp).

Author Contributions: Drs Kashio, Ito, Karino, Iwasaki, Sakamoto, Suzuki, and Yamasoba had full access to all the data in the study and take responsibility for the integrity of the data and the accuracy of the data analysis. *Study concept and design:* Kashio and Ito. *Acquisition of data:* Kashio, Ito, Karino, Iwasaki, Sakamoto, Suzuki, and Yamasoba. *Analysis and interpretation of data:* Kashio, Ito, Kakigi, Sakamoto, Yasui, and Yamasoba. *Drafting of the manuscript:* Kashio, Ito, and Yasui. *Critical revision of the manuscript for important intellectual content:* Kashio, Ito, Kakigi, Karino, Iwasaki, Sakamoto, Suzuki, and Yamasoba. *Statistical analysis:* Ito and Yasui. *Administrative, technical, and material support:* Kashio. *Study supervision:* Ito, Kakigi, Karino, Iwasaki, Sakamoto, Suzuki, and Yamasoba.

Financial Disclosure: None reported.

REFERENCES

1. Carhart R. Clinical application of bone conduction audiometry. *Arch Otolaryngol.* 1950;51(6):798-808.
2. Yasan H. Predictive role of Carhart's notch in pre-operative assessment for middle-ear surgery. *J Laryngol Otol.* 2007;121(3):219-221.
3. Ahmad I, Pahor AL. Carhart's notch: a finding in otitis media with effusion. *Int J Pediatr Otorhinolaryngol.* 2002;64(2):165-170.
4. Conijn EA, Van der Drift JF, Brocaar MP, Van Zanten GA. Conductive hearing loss assessment in children with otitis media with effusion: a comparison of pure tone and BERA results. *Clin Otolaryngol Allied Sci.* 1989;14(2):115-120.
5. Browning GG, Gatehouse S. Hearing in chronic suppurative otitis media. *Ann Otol Rhinol Laryngol.* 1989;98(4, pt 1):245-250.
6. Dumich PS, Harner SG. Cochlear function in chronic otitis media. *Laryngoscope.* 1983;93(5):583-586.
7. Tüz M, Doğru H, Uygur K, Gedikli O. Improvement in bone conduction threshold after tympanoplasty. *Otolaryngol Head Neck Surg.* 2000;123(6):775-778.
8. Kirikae I. An experimental study on the fundamental mechanism of bone conduction. *Acta Otolaryngol Suppl.* 1959;145:1-111.
9. Tonndorf J, Campbell R, Bernstein L, Reneau JI. Quantitative evaluation of bone conduction components in cats. *Acta Otolaryngol Suppl.* 1966;213:10-38.

10. Lam HY. Causes of hearing disorders. In: Kerr AG, ed. *Scott-Brown's Otolaryngology Adult Audiology*. 6th ed. Oxford, England: Butterworth-Heinemann; 1996: 2.10.1-2.10.28.
11. Dirks DD. Bone-conduction testing. In: Katz J, ed. *Handbook of Clinical Audiology*. 3rd ed. Baltimore, MD: Williams & Wilkins; 1985.
12. Naunton RF, Fernandez C. Prolonged bone conducton: observations on man and animals. *Laryngoscope*. 1961;71:306-318.
13. Huizing EH. Bone conduction—the influence of the middle ear. *Acta Otolaryngol Suppl*. 1960;155:1-99.
14. Goodhill V. The fixed malleus syndrome. *Trans Am Acad Ophthalmol Otolaryngol*. 1966;70(3):370-380.
15. Dirks DD, Malmquist GM. Comparison of frontal and mastoid bone-conduction thresholds in various conductive lesions. *J Speech Hear Res*. 1969;12(4):725-746.
16. Priede V. Acoustic impedance in two cases of ossicular discontinuity. *Int Audiol*. 1970;1:127-136.
17. Linstrom CJ, Silverman CA, Rosen A, Meiteles LZ. Bone conduction impairment in chronic ear disease. *Ann Otol Rhinol Laryngol*. 2001;110(5 Pt 1):437-441.
18. Barany E. A contribution to the physiology of bone conduction. *Acta Otolaryngol Suppl*. 1938;26:1-223.
19. Allen GW, Fernandez C. The mechanism of bone conduction. *Ann Otol Rhinol Laryngol*. 1960;69:5-28.
20. Stenfelt S. Middle ear ossicles motion at hearing thresholds with air conduction and bone conduction stimulation. *J Acoust Soc Am*. 2006;119(5, pt 1):2848-2858.
21. Ginsberg IA, Hoffman SR, Stinziano GD, White TP. Stapedectomy—in depth analysis of 2405 cases. *Laryngoscope*. 1978;88(12):1999-2016.
22. Stenfelt S, Goode RL. Bone-conducted sound: physiological and clinical aspects. *Otol Neurotol*. 2005;26(6):1245-1261.
23. Tsai V, Ostroff J, Korman M, Chen JM. Bone-conduction hearing and the occlusion effect in otosclerosis and normal controls. *Otol Neurotol*. 2005;26(6): 1138-1142.
24. Moller AR. *Hearing: Its Physiology and Pathophysiology*. San Diego, CA: Academic Press; 2000.
25. Àwengen DF. Change of bone conduction thresholds by total footplate stapedectomy in relation to age. *Am J Otolaryngol*. 1993;14(2):105-110.
26. Gerard JM, Serry P, Gersdorff MC. Outcome and lack of prognostic factors in stapes surgery. *Otol Neurotol*. 2008;29(3):290-294.
27. Cook JA, Krishnan S, Fagan PA. Quantifying the Carhart effect in otosclerosis. *Clin Otolaryngol Allied Sci*. 1995;20(3):258-261.

Behavioral/Systems/Cognitive

Axonal Branching Patterns as Sources of Delay in the Mammalian Auditory Brainstem: A Re-Examination

Shotaro Karino,[1,4] Philip H. Smith,[2] Tom C. T. Yin,[3] and Philip X. Joris[1]

[1]Laboratory of Auditory Neurophysiology, Medical School, University of Leuven, B-3000 Leuven, Belgium, Departments of [2]Anatomy and [3]Physiology, University of Wisconsin–Madison, Madison, Wisconsin 53706-1510, and [4]Department of Otolaryngology, Faculty of Medicine, University of Tokyo, Tokyo 113-8655, Japan

In models of temporal processing, time delays incurred by axonal propagation of action potentials play a prominent role. A pre-eminent model of temporal processing in audition is the binaural model of Jeffress (1948), which has dominated theories regarding our acute sensitivity to interaural time differences (ITDs). In Jeffress' model, a binaural cell is maximally active when the ITD is compensated by an internal delay, which brings the inputs from left and right ears in coincidence, and which would arise from axonal branching patterns of monaural input fibers. By arranging these patterns in systematic and opposite ways for the ipsilateral and contralateral inputs, a range of length differences, and thereby of internal delays, is created so that the ITD is transformed into a spatial activation pattern along the binaural nucleus. We reanalyze single, labeled, and physiologically characterized axons of spherical bushy cells of the cat anteroventral cochlear nucleus, which project to binaural coincidence detectors in the medial superior olive (MSO). The reconstructions largely confirm the observations of two previous reports, but several features are observed that are inconsistent with Jeffress' model. We found that ipsilateral projections can also form a caudally directed delay line pattern, which would counteract delays incurred by caudally directed contralateral projections. Comparisons of estimated axonal delays with binaural physiological data indicate that the suggestive anatomical patterns cannot account for the frequency-dependent distribution of best delays in the cat. Surprisingly, the tonotopic distribution of the afferent endings indicate that low characteristic frequencies are under-represented rather than over-represented in the MSO.

Introduction

Coincidence detectors and time delays are common ingredients in models of temporal processing. In such models, neural equivalents of cross-correlation or autocorrelation are implemented by comparing spike trains with delayed versions of themselves or with other spike trains. A pre-eminent example is in binaural hearing, which affords the detection of minute time differences in the sound signals to the two ears [interaural time differences (ITDs)] that contain information about the spatial properties of sound sources. Neuronal ITD sensitivity in mammals originates in the medial superior olive (MSO). For >50 years, one model (Jeffress, 1948) has dominated the discussion of the neural mechanisms of ITD discrimination and its relationship to MSO activity. In this model, a binaural cell shows a "best delay": it is maximally active when the external acoustic delay (the ITD) is compensated by an internal delay, so that the inputs from left and right ear to the cell are coincident. Classic studies of ITD sensitivity (Rose et al., 1966; Goldberg and Brown, 1969; Yin and Chan, 1990) provided evidence for coincidence in accord with the Jeffress (1948) model (Joris et al., 1998; Joris, 2006). Jeffress hypothesized the source of internal delays as axonal length differences. He proposed that afferent axons are systematically arranged with length gradients in opposite directions for ipsilateral (Ipsi) and contralateral (Contra) inputs to an array of coincidence detectors. The result would be a systematic gradation in best delay along the binaural nucleus and the conversion of ITDs into a spatial activation pattern along the array.

In mammals, only two studies have examined the existence of delay lines anatomically. Smith et al. (1993) physiologically characterized and then labeled single afferent axons to the MSO from spherical bushy cells of the anteroventral cochlear nucleus (AVCN). They concluded that the projections to the contralateral MSO, but not the ipsilateral MSO, display a rostrocaudal (RC) delay line configuration. Beckius et al. (1999) labeled small populations of AVCN neurons with an extracellular deposit, and selected and reconstructed individual axons. Their results were similar to those of Smith et al. (1993) with the additional finding of a length gradient running in the opposite (caudorostral) direction in some ipsilateral projections. Physiologically, MSO neurons show a rostrocaudal gradient in ITD tuning consistent with the anatomical predictions (Yin and Chan, 1990).

Despite the anatomical and physiological support, the Jeffress (1948) model is no longer universally accepted for mammals (Palmer, 2004; McAlpine, 2005; Palmer and Kuwada, 2005; Joris

Received Oct. 1, 2010; revised Dec. 1, 2010; accepted Dec. 30, 2010.

This work was supported by the Fund for Scientific Research–Flanders (Grants G.0392.05 and G.0633.07 to P.J.; Fellowship GP.037.07N to S.K.), Research Fund K.U. Leuven (Grants OT/05/57 and OT/09/50 to P.J.; Fellowship F/06/085 to S.K.), the National Institutes of Health (Grant DC00116 to T.Y.), and the National Science Foundation (Grant BNS-8901993 to P.S.).

The authors declare no competing financial interests.

Correspondence should be addressed to Philip X. Joris, Laboratory of Auditory Neurophysiology, Campus Gasthuisberg O&N 2, Herestraat 49, bus 1021, B-3000 Leuven, Belgium. E-mail: Philip.Joris@med.kuleuven.be.

DOI:10.1523/JNEUROSCI.5175-10.2011

 0270-6474/11/313016-16$15.00/0

and Yin, 2007), while it remains unchallenged in the barn owl (Wagner et al., 2007). McAlpine et al. (1996, 2001) discovered a relationship between best delay and frequency tuning in binaural neurons, which is not necessarily contradictory to the Jeffress (1948) model but certainly is not predicted by it. Moreover, the anatomical evidence for delay lines in the mammal has been questioned (Grothe, 2003). Our purpose here is to re-examine the data of Smith et al. (1993) quantitatively and to examine the anatomical data in the light of the more recently discovered relationship between ITD tuning and frequency tuning.

Materials and Methods

Material. The surgical procedure, stimulus delivery, and physiological and histological methods are described in the original study (Smith et al., 1993) and are only briefly outlined here. We will focus on the quantitative, computerized processing of the fibers labeled.

The ventral brainstem was exposed in cats of either sex, anesthetized with sodium pentobarbital. Sharp electrodes filled with either a 5% horseradish peroxidase (HRP) (type VI, Sigma) or 2% neurobiotin (Vector Laboratories) solution in 0.5 M KCl were advanced into the trapezoid body while presenting calibrated search tones. When a fiber was isolated, the excitatory ear, the characteristic frequency (CF), spontaneous activity, and threshold at CF were determined by an automated threshold tracking program. Poststimulus time histograms for short (25 ms) tones at CF were then obtained at different sound pressure levels (in 10 or 20 dB steps) usually up to 50–60 dB above threshold. Intra-axonal impalement was achieved with current pulses or electrode advancement, followed by confirmation of the physiological responses. HRP or neurobiotin was then injected by iontophoresis. After 24–36 h, a lethal dose of sodium pentobarbital was given and the animal was perfused transcardially with phosphate-buffered glutaraldehyde/paraformaldehyde fixative.

For preparation of HRP-filled axons, frozen or vibratomed 60 or 70 μm sections of the brainstem were processed using the DAB nickel–cobalt intensification method (Adams, 1981). For preparation of neurobiotin-filled cells, the sections were washed in 0.1 M phosphate buffer, incubated for 20 min in 0.5% H_2O_2, rinsed in PBS, and left overnight in phosphate buffer containing avidin-biotin-HRP reagent (ABC kit, Vector Laboratories). The sections were then rinsed in buffer, treated with DAB (as above), mounted on glass slides, counterstained with cresyl violet, and coverslipped.

Reconstructions and analysis. Because the axons typically extended over many coronal sections, detailed analysis and three-dimensional reconstructions required computer reconstruction. We used a Neurolucida system (Microbrightfield) that included an Olympus BX61 light microscope, a video camera (MBF-CX9000, Microbrightfield), a motorized stage controller (MAC5000, Ludl Electronic Products), and a personal computer. Axons were traced and digitized directly on the microscope using a UPlanFLN 40× objective. The (x,y,z) positions accompanied with axon diameter were collected every 1.9 μm on average (538 points/mm). Section thickness measured with the microscope z-axis ranged from 20 to 25 μm. Corrections were made for shrinkage along this axis (i.e., the rostrocaudal direction) according to the section thickness specified during cutting and the thickness measured in the microscope. Estimates of axon diameter were made by adjusting the diameter of a circular cursor to the width of the labeled axon and do not include the myelin sheath. For several reasons, stated in Smith et al. (1993), these measurements should be regarded as coarse estimates.

The furthest distal points that could be traced were defined as endpoints (EPs; for ease of reading we use the full words in the text and the abbreviations in figures). These points are not identical to terminals: the darkness of the label typically decreased with distance from the injection site and toward the middle of the sections, so that the finest processes could not always be followed to unambiguous terminations. Moreover, all of the reconstructions analyzed here were done with the light microscope, so we cannot be sure that the afferent endpoints terminate at a synapse. However, we have analyzed a small number of the labeled axons with the electron microscope, and the afferent terminals were confirmed to be presynaptic (Smith et al., 1991, 1993). Also, comparison with Beckius et al. (1999) (see Results) suggests that our tracings must have covered the axons almost in their entirety in many cases. Importantly, the sheet-like mammalian MSO has limited thickness, and the delay line configuration is thought to span the rostrocaudal dimension: the main contributors to differential length are not the terminal axonal segments but rather the more proximal main stem of the axon, which gives off branches at different rostrocaudal positions (see Figs. 2*C*, 3). Assessment of collateral length differences along the rostrocaudal axis thus does not hinge on complete filling to the axon terminals.

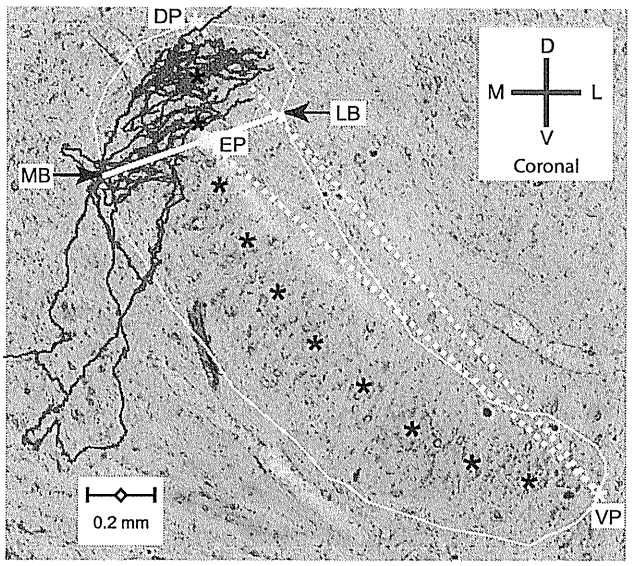

Figure 1. Illustration of measurements taken within sections. Coronal view of the contralateral projection of a traced fiber (CF, 1345 Hz) superimposed on a Nissl-stained single section, taken at the coronal level of the branch EP, indicated with the yellow dot. Yellow line, Contour of MSO on the section. Yellow asterisks, Most DP and most VP along the long axis of the MSO within the section, which is indicated with black asterisks. Drawing a line through the EP, which is approximately perpendicular to the long axis of the MSO, the arrows show the most medial and lateral points (MB and LB) of the MSO contour on this line. The two other lines (dotted white) indicate the Euclidian distances between EP and VP, and between VP and the DP of this section. Scale bar, 200 μm. Directions are indicated by the cross. D, Dorsal; V, ventral; M, medial; L, lateral.

We defined several markers to take measurements for numerical analysis. Figure 1 illustrates markers defined within single sections. The yellow line traces the MSO contour, and the black asterisks its long axis within the section. The yellow asterisks indicate the dorsal pole (DP) and ventral pole (VP). These are not necessarily literally the extreme dorsal and ventral points of the MSO outline in that section. For example, the ventral pole in Figure 1 is not the most ventral point of the MSO. Rather, dorsal pole and ventral pole are the extreme ends of the—often curved—long axis of the MSO within the section. The yellow disk marks one endpoint (EP). To express the dorsoventral location of an endpoint within the MSO, we measured its Euclidian distance to the ventral pole, which we normalized to the Euclidian distance between dorsal pole and ventral pole (Fig. 1, dotted white lines). Normalization facilitates comparison across animals as it reduces variance resulting from differences in absolute dimensions of the MSO. Values close to 1 indicate an endpoint located close to the dorsal pole; values close to 0 indicate a position close to the ventral pole. We also measured the mediolateral location of endpoints based on their distance to the edge of the MSO outline, taken at the intersection of the outline with a line (Fig. 1, solid white line) that is approximately orthogonal to its long axis. These intersections give two measurements for each endpoint: the medial border (MB) and the lateral border (LB). These latter measurements are inherently coarse, particularly for endpoints close to the dorsal or ventral pole of the MSO. Again, we normalized the midline (ML) position as the (Euclidian distance between endpoint and medial border)/(Euclidian distance between lat-

eral border and medial border). When this value is close to 1, the endpoint is located close to the lateral border.

Measurements taken across sections are illustrated in Figure 2 in the coronal (Fig. 2*A*), horizontal (Fig. 2*B*), and parasagittal (Fig. 2*C*) planes, for the same fiber used in Figure 1. First, the most rostral and most caudal sections where the MSO could be discerned are identified. The geometrical centers of the MSO outlines in these sections (Fig. 2*A*, green and magenta) were designated as the rostral pole (RP) and caudal pole (CP). The normalized RC distance of an endpoint relative to these poles was measured as (Euclidian distance between endpoint and rostral pole)/(Euclidian distance between caudal pole and rostral pole), illustrated with the dotted lines (Fig. 2*B*,*C*). An endpoint close to the caudal pole thus gives an RC value close to 1. For contralateral projections, we also marked the point where the axon crossed the ML. Finally, for both ipsilateral and contralateral projections we marked the first branch point (FB) (i.e., the last point of the axon that is common for all branches to the ipsilateral or contralateral MSO) (Fig. 2*B*,*C*). The axonal length from midline or first branch point to each endpoint was calculated as the sum of the distances between adjacent (*x*,*y*,*z*) coordinates in the course of the axon to that endpoint.

For the sake of brevity, we use the shorthand "delay line" to refer to a morphological pattern of systematic length differences in axon collaterals. We caution that the term inherently refers to a functional concept that can only be validated with physiological measurements—a point to which we will return in Discussion.

Results

The material we analyzed here consists of 14 labeled fibers, obtained from 12 animals. We reconstructed the 16 projections (9 contralateral, 7 ipsilateral) reported in Smith et al. (1993). For only two fibers (with CFs of 1498 Hz and 2470 Hz) were both contralateral and ipsilateral projections sufficiently labeled for reconstruction. A qualitative description of the course and projections of the fibers is provided in Smith et al. (1993) and is summarily illustrated here for several fibers. We identify projections with the same number, symbol, and color scheme in all figures, where relevant.

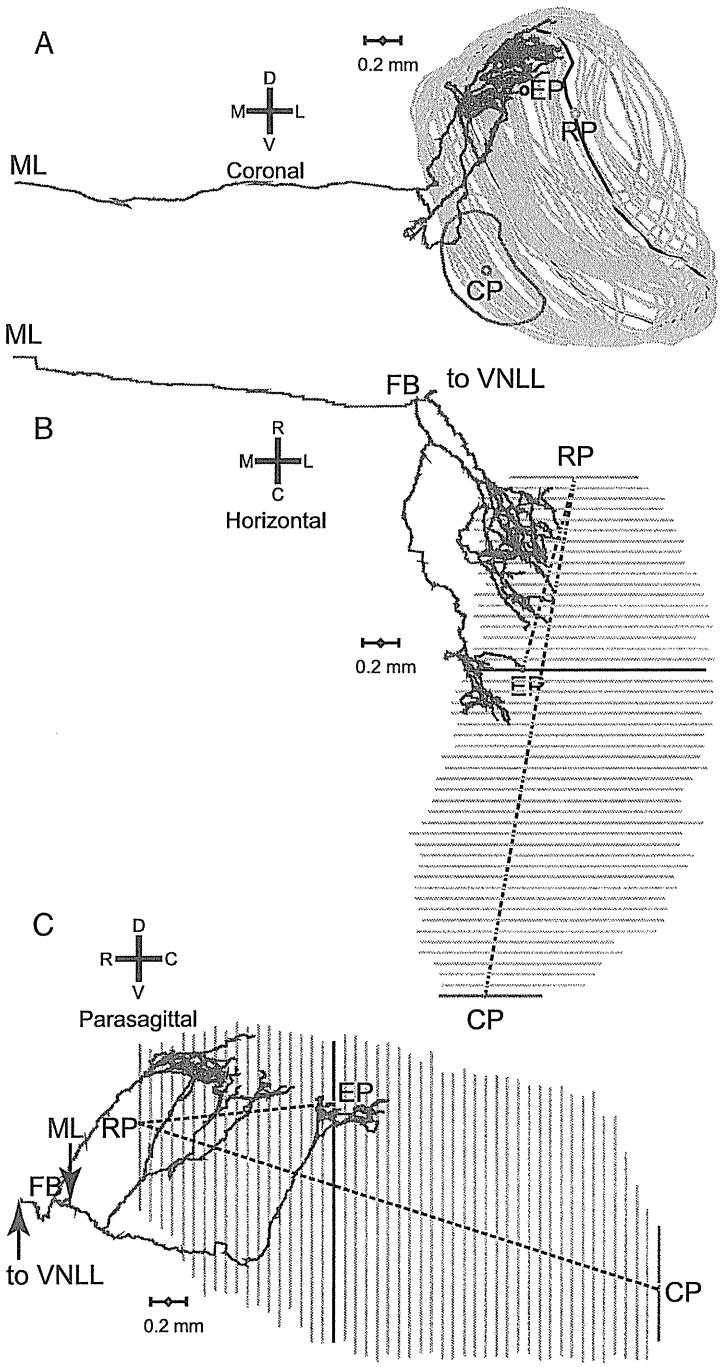

Figure 2. Example of the contralateral MSO innervation by one axon (same axon as in Fig. 1). ***A–C***, Coronal (***A***), horizontal (***B***), and parasagittal (***C***) views are shown. The RP and CP were defined as the geometrical center of the most rostral (green line) and most caudal (magenta line) section, respectively. The rostrocaudal position of endpoints was quantified by measuring the Euclidian distance (dashed line) between RP and EP, and was normalized to the distance between RP and CP. The endpoint illustrated is the same one as in Figure 1; the MSO contour outlined in Figure 1 is shown in blue here. ML indicates the point at which the axon crosses the midline. CF of this fiber was 1345 Hz. A computer reconstruction of this fiber was also shown in Smith et al. (1993, their Fig. 4).

Contralateral projections

Nine contralaterally injected fibers were well labeled and used for the analyses. The axon in Figure 2 crossed the midline at a level rostral to the MSO and projected multiple collateral branches caudally before heading rostrally toward the ventral nucleus of the lateral lemniscus (VNLL). The collateral projections span approximately half of the rostral-caudal extent of the MSO nucleus with a ladder-like branching pattern that is particularly clear in the parasagittal view (Fig. 2*C*). Similar innervation patterns are shown for three fibers in Figure 3. The axons in Figure 3, *A* and *B*, also cross the midline in a rostral position and give caudally directed branches over a more restricted (Fig. 3*A*) or less restricted (Fig. 3*B*) rostrocaudal distance than in Figure 2. The axon in Figure 3*C*, shown in horizontal view, crosses the midline at a more caudal level. It shows three branches that are directed to the central and caudal MSO, as well as one branch

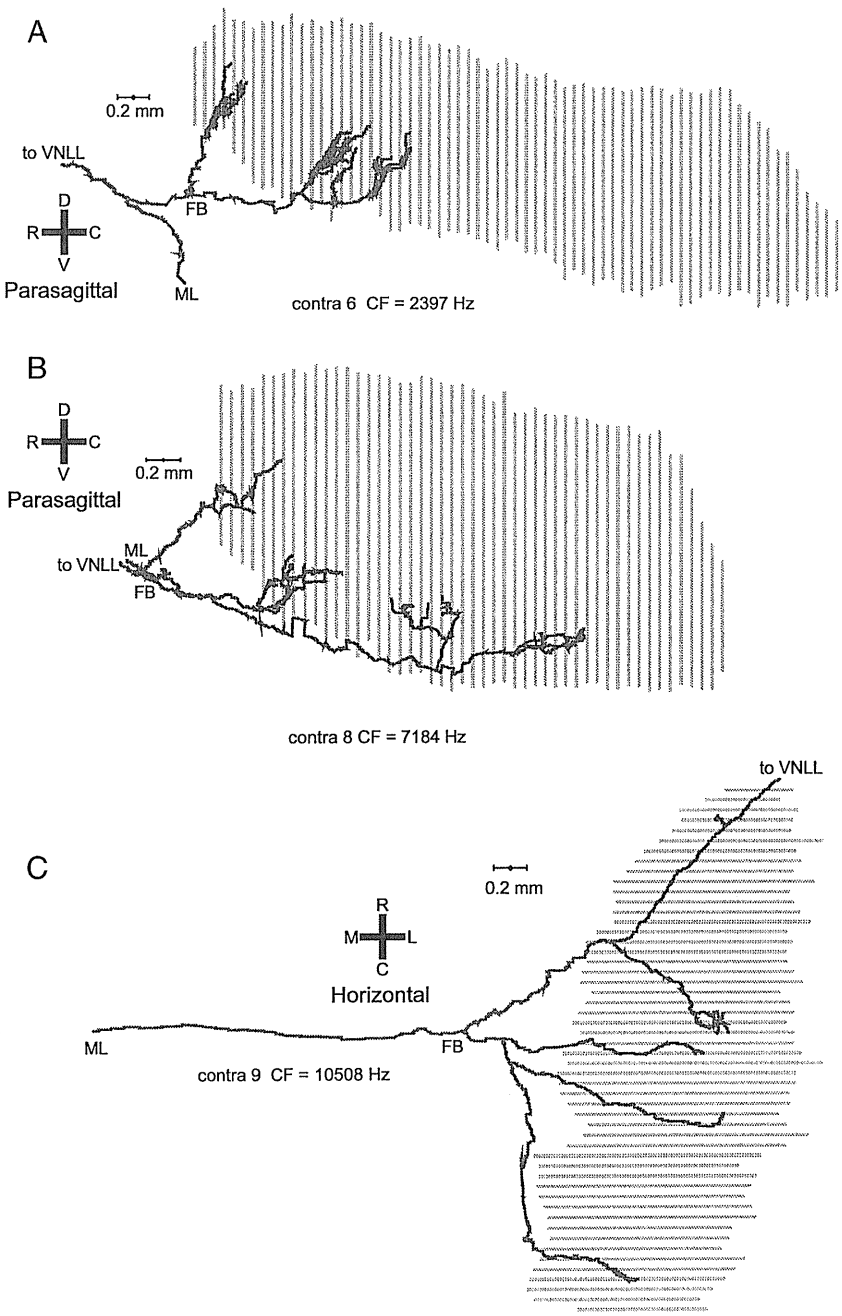

Figure 3. Delay line configuration in 3 contralaterally projecting fibers. ***A***, ***B***, Projections on a parasagittal plane. ***C***, Projection on a horizontal plane. CFs are indicated. Branches that end within the MSO are indicated in red.

that is directed rostrally and does not seem to fit the caudally directed delay line patterns of the fibers discussed so far. A similar case is shown in parasagittal view in Figure 4*A*. The axon also crosses the midline at a rostrocaudal position that bisects the MSO in approximately equal halves. It shows a number of caudally directed collateral branches with increasing length, but also a branch that innervates the rostral half of the MSO and continues on toward the VNLL. Fibers that reach the MSO at an even more caudal position are shown in Figure 4, *B* and *C*. The fiber in Fig. 4*B* has a rostrocaudally restricted field. The axon in Fig. 4*C* shows no obvious bias toward increasing length for more caudally projecting collaterals.

Ipsilateral projections

Seven ipsilaterally injected fibers were adequately labeled for our analyses. Because the pattern of the ipsilateral projections is more complicated than that of the contralateral projections described above, we show the projections in different views. The fiber illustrated in Figure 5 had several collaterals without an obvious delay line pattern. Two types of collateral projections can be distinguished: forward and backward. The coronal view (Fig. 5*A*) shows one branch coursing along the lateral aspect of the MSO (forward innervation), consistent with the known segregation of ipsilateral and contralateral inputs to the lateral and medial dendrites of MSO neurons, respectively (Stotler, 1953). Two more collaterals only branch off from the main axon after it has crossed underneath the MSO, to then loop back through the MSO to innervate the same region (backward innervation). These branches have their origins medial to the ipsilateral MSO. All of the seven ipsilateral projections had "backward" components; four of the seven ipsilateral projections had "forward" components (Fig. 10*B*, summary).

Figure 6 shows another example of an ipsilateral projection. In this case, the forward and backward innervation contribute endpoints that are located at different rostrocaudal positions (Fig. 6*B*,*C*), where the backward branches innervate a more rostral part of the MSO than the forward branches. The horizontal and parasagittal views suggest that this fiber has greater length in its caudal than in its rostral innervation, but the complex course of the branches in the three dimensions precludes a simple visual assessment. In fact, length measurements reveal greater length in the rostral than in the caudal innervation (see Fig. 8*D*, green inverted triangles).

Dendrograms

Because branches often extensively overlap in the projections of the computer reconstructions in Figures 1–6, these views do not give an adequate representation of the complexity of branching. Figure 7 gives an overview, for the most completely filled fibers, of the sequence of branchings in contralateral (left column) and ipsilateral (right column) projections. The horizontal axis indicates the length of segments bordered by midline, branch points, or endpoints. The vertical axis only serves to offset the different segments after branching: it does not have the physical meaning of length, and there is no vertical sorting according to position in the MSO. The dendrograms therefore provide information about branch sequence and length (abscissa), but they contain no anatomical directional information (e.g., lateral vs medial, dorsal vs ventral, rostral vs caudal). There is obviously profuse branching in both contralat-